ELSEVIER

Nuclear Instruments and Methods in Physics Research A 424 (1999) 512–522

NUCLEAR INSTRUMENTS & METHODS IN PHYSICS RESEARCH Section A

Surface field in an ensemble of superconducting spheres under external magnetic field

A. Peñaranda*, C.E. Auguet, L. Ramírez-Piscina

Departament de Física Aplicada, Universitat Politècnica de Catalunya, Avda. Gregorio Marañón 44, E-08028 Barcelona, Spain

Received 25 June 1998

Abstract

We perform calculations of the magnetic field on the surface of an ensemble of superconducting spheres when placed into an external magnetic field, which is the configuration employed in superheated superconducting granule detectors. The Laplace equation is numerically solved with appropriate boundary conditions by means of an iterative procedure and a multipole expansion.

Keywords: Superconducting spheres; Laplace equation; Multipole expansion; Lattice spacings

1. Introduction

Detectors based on the phase transition of superheated superconducting granules induced by the energy loss of incident radiation are currently under development for the detection of neutrinos and dark matter [1,2]. They have been further proposed as sensors for many types of particles, including γ-rays, X-rays, electrons, neutrons and neutrinos [3–9], transition radiation [6,10], and magnetic monopoles [11]. In these devices, a dispersion of a large number of superconducting, micrometric spheres are maintained in a metastable state below T_c by an external magnetic field. First-order transitions from the superconducting-to-normal state are sensed via the flux change resulting from the accompanying loss of the Meissner state, which induces a pulse on a surrounding wire loop to provide the interaction signal.

The energy required to induce a phase transition depends on the location of a grain within the (T, H) phase space as shown in Fig. 1, which depends on the inherent variation of the individual local fields resulting from the distribution of sizes, defects and diamagnetic interactions between the grains. These effects yield a typically 20% spreading of the transition fields of the ensemble, generating difficulties in interpreting the results of device response [3–6]. Since increase of distances between grains reduces the effects of the diamagnetic interactions, ordered arrays of spherical indium grains produced from thin films deposited on mylar foils using photolithographic techniques have been explored; although such PASS devices [12] have yielded differential superheating curves with the field

* Corresponding author. Tel.: + 34934016263; fax: + 349 34017700; e-mail: angelina@hal9000.upc.es.

0168-9002/99/$ – see front matter
PII: S0168-9002(98)01440-5

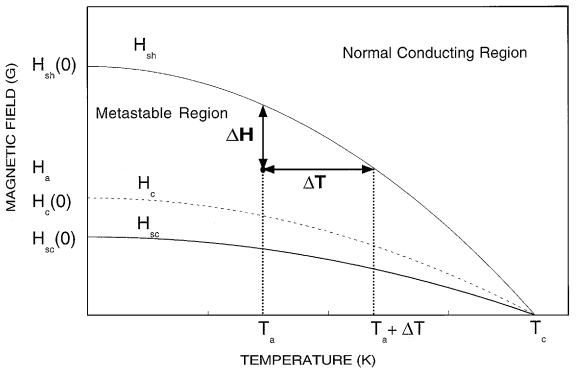

Fig. 1. Phase diagram for a type I superconductor. ΔH and ΔT represent the increase of either the magnetic field or the temperature needed for a metastable superconductor grain at H_a, T_a to transite.

spreading reduced by an order of magnitude, they have not eliminated it.

A point often neglected in recent analyses of the device response to irradiation is that the local grain magnetic fields are not static, but evolve with time as grains transition. Moreover, all response studies are conducted at fixed magnetic threshold above the thermodynamic critical field, for which some fraction of the ensemble is already in the normal state. An important aspect of the understanding of the basic device response is thus the knowledge of the variation of the local magnetic field at the surface of the superconducting granules in the presence of the ensemble-modified external field, and in particular its maximum value. Calculations involving magnetostatic interactions between many bodies turns out to be far from trivial. The first theoretical analyses of this problem treated the dielectric interactions between spheres in a dipolar and two-body approximation [13,14] and hence with a validity limited to very low densities. The most systematic effort in the interpretation of experimentals has so far been the perturbative analyses of Geigenmüller [15,16], which yielded results on the succesive transitions of the spheres when the magnetic field is increased from zero. This calculation is based on a cluster expansion, and was performed up to the first order in the volume filling factor, which implies only pair interactions between the spheres.

The aim of this paper is to perform a fixed, low-field analysis of the system which is not limited to low densities, as a first step towards a more complete analyses of the magnetic response. This involves the complete resolution of the Laplace equation under the boundary conditions given by the presence of a large number of diamagnetic spheres and an external field. In Section 2 we perform such calculations by a multipole expansion and iterative procedure, which permits one in principle to reach any arbitrary precision in a systematic way. In practice, we obtain the maximum surface field on the spheres with a precision of order 1% for ensembles up to 150 superconducting spheres, and for occupied volume fractions up to 20% with a reasonable computational effort.

In Sections 3 and 4 we present numerical results for the two typical configurations. The first, which we refer to as "disordered", is the traditional suspension of superconducting micrometric spheres homogeneously diluted in parafin wax by repeated baker's transformations [17]. The second configuration, which we call "regular", corresponds to the PASS structure [12]: the spheres are placed in 2D and 3D square lattices of variable cell length d. Finally, we present conclusions in Section 5.

2. Numerical method

For the sake of simplicity we assume that the granules are perfect spheres (of radius much larger than the London penetration length) and that the superconducting-to-normal transition of each granule is complete when the surface field reaches some threshold value. Therefore, we do not account for the experimentally observed case of partially superconducting intermediate states. This hypothesis is justified when the local magnetic field applied over a sphere is greater than the critical magnetic field B_c, and thus the sphere is in a metastable state [15].

We consider an ensemble of N spheres of radius a with positions given by $\boldsymbol{R}_i$. The magnetic field $\boldsymbol{B}(\boldsymbol{r})$ can be written in terms of a scalar potential $U(\boldsymbol{r})$:

$$\boldsymbol{B}(\boldsymbol{r}) = -\nabla U(\boldsymbol{r}), \tag{2.1}$$

which satisfies the Laplace equation

$$\nabla^2 U(\boldsymbol{r}) = 0. \tag{2.2}$$

Two boundary conditions apply. First the magnetic field is tangent to the surface of any superconducting sphere, i.e. the normal derivative of the potential vanishes there. Secondly, the value of the field very far from the sample should match $\boldsymbol{B}_{\text{ext}}$:

$$U(\boldsymbol{r}) \to -\boldsymbol{r}\cdot\boldsymbol{B}_{\text{ext}} \quad (r \to \infty). \tag{2.3}$$

We start from the formal resolution of the Laplace equation in the presence of superconducting spheres due to Geigenmüller [15,16]. The scalar potential $U(\boldsymbol{R}_j + \boldsymbol{r}_j)$ near sphere j is expanded in multipoles, which with the boundary conditions at the surface of the sphere can be written as

$$U(\boldsymbol{R}_j + \boldsymbol{r}_j) = \sum_{\lambda=1}^{\infty} \sum_{\mu=-\lambda}^{\lambda} Y_{\lambda\mu}(\hat{r}_j)\, c_{\lambda\mu}(j) \times \left\{ \left(\frac{a}{r_j}\right)^{\lambda+1} + \frac{\lambda+1}{\lambda}\left(\frac{r_j}{a}\right)^{\lambda} \right\} + K(j), \tag{2.4}$$

where $Y_{\lambda\mu}(\hat{r}_j)$ are the spherical harmonics, and $c_{\lambda\mu}(j)$ and $K(j)$ are the coefficients of the expansion. There is one of these expansions for each sphere.

The problem is now only to find the unknowns $c_{\lambda\mu}(j)$ and $K(j)$ for a given configuration. Once these constants are known, one can calculate the surface fields from Eq. (2.4). The matching of all of these expansions to each other and to the boundary condition at infinity gives the following equations [16]:

$$K(j) = -\boldsymbol{R}_j\cdot\boldsymbol{B}_{\text{ext}} + \sum_{k\neq j} \sum_{\lambda=1}^{\infty} \sum_{\mu=-\lambda}^{\lambda} A_{00\,\lambda\mu}(j,k)\, c_{\lambda\mu}(k), \tag{2.5}$$

$$\frac{\lambda+1}{\lambda} c_{\lambda\mu}(j) = -\sqrt{\frac{4\pi}{3}} B_{\text{ext}} a\, \delta_{\lambda 1}\delta_{\mu 0} + \sum_{k\neq j} \sum_{\lambda'=1}^{\infty} \sum_{\mu'=-\lambda'}^{\lambda'} A_{\lambda\mu\,\lambda'\mu'}(j,k) c_{\lambda'\mu'}(k), \tag{2.6}$$

where the constants $A_{\lambda\mu\lambda'\mu'}(j,k)$ are

$$A_{\lambda\mu\lambda'\mu'}(j,k) = \sum_{\mu''=-\lambda_0}^{\lambda_0} (-1)^{\lambda'+\mu''} \times \left[\frac{2\lambda'+1}{2\lambda+1}\binom{\lambda+\lambda'}{\lambda+\mu''}\binom{\lambda+\lambda'}{\lambda'+\mu''}\right]^{1/2} \times D^{\lambda}_{\mu\mu''}(\varphi_{R_{jk}}, \theta_{R_{jk}}, 0)\, D^{\lambda'}_{\mu''\mu'}(0, -\theta_{R_{jk}}, -\varphi_{R_{jk}}) \times \left(\frac{a}{R_{jk}}\right)^{\lambda+\lambda'+1} (\lambda_0 = \min(\lambda,\lambda')). \tag{2.7}$$

The $(R_{jk},\theta_{R_{jk}},\varphi_{R_{jk}})$ are the polar coordinates of $\boldsymbol{R}_{jk} = \boldsymbol{R}_k - \boldsymbol{R}_j$, and

$$D^{\lambda}_{\mu\mu'}(\alpha,\beta,\gamma) = \mathrm{e}^{-\mathrm{i}(\mu\alpha+\mu'\gamma)}[(\lambda+\mu)!(\lambda-\mu)!(\lambda+\mu')!(\lambda-\mu')!] \times \sum_{\lambda'} \frac{(-1)^{\lambda'}}{(\lambda-\mu-\lambda')!(\lambda+\mu'-\lambda')!(\lambda'+\mu-\mu')!\lambda'!} \times \left(\cos\frac{\beta}{2}\right)^{2\lambda+\mu'-\mu-2\lambda'} \left(-\sin\frac{\beta}{2}\right)^{\mu-\mu'+2\lambda'}. \tag{2.8}$$

Without loss of generality in Eq. (2.6), we have placed the external field in the z-direction.

The constants $K(j)$ only give additive contributions to the potential and do not affect the magnetic field values, so one has in principle to solve the infinite set of linear equations (2.6) for the unknown c's. In view of Eq. (2.7) the constants $A_{\lambda\mu\lambda'\mu'}(j,k)$ are of order $(a/R_{jk})^{\lambda+\lambda'+1}$ where R_{jk} is the distance between spheres. Thus one can safely cut the expansion of Eq. (2.4) to some $\lambda_{\max}$ according to the desired precision, and Eq. (2.6) reduces to a finite set of linear equations.

However, the great number of complex unknowns that appear have so far prevented the application of this method for actual simulations with reasonable values of N. For example, for $N = 100$ and $\lambda_{\max} = 10$, the number M of complex unknowns is of order $N\lambda_{\max}^2 = 10^4$. Direct numerical methods (matrix inversion, LU decomposition, etc) are not suitable in such a large linear system of equations, because of lack of precision [18], memory usage (the matrix of coefficients is $M \times M$) and CPU time (of order M^3). In such cases one must

rely on some kind of iterative method. We observe that Eq. (2.6) can formally be written as a matrix equation for the vector of unknowns $\boldsymbol{c}$:

$$\boldsymbol{c} = \boldsymbol{b} + A\boldsymbol{c} \tag{2.9}$$

whose solution is

$$\boldsymbol{c} = (I - A)^{-1}\boldsymbol{b}, \tag{2.10}$$

which can be written as a power series in A,

$$\boldsymbol{c} = (I + A + A^2 + A^3 + \cdots)\boldsymbol{b}. \tag{2.11}$$

The easiest way to numerically perform this expansion is to apply the iteration

$$\boldsymbol{c}_{i+1} = \boldsymbol{b} + A\boldsymbol{c}_i, \tag{2.12}$$

$$\boldsymbol{c}_0 = \boldsymbol{b}. \tag{2.13}$$

The largest matrix elements of A are of order $(a/R)^3$ with R of order the distance between spheres: the expansion is guaranteed to converge, and this convergence should be faster for more diluted systems. One can repeat Eq. (2.12) until the change of the coefficients c is lower than some given value. For our typical simulations, changes lower than 0.5% are achieved for about four iterations. In this procedure the CPU time scales as M^2 and it is not necessary to maintain the whole matrix A in memory.

The simulation procedure is the following: once the spheres have been placed according to the desired geometry, we iterate Eq. (2.12) until the desired precision is achieved. The resulting values of the c's are employed to derive from Eqs. (2.1) and (2.4) the local values of the magnetic field at the sphere surface ($r_j = a$). We then calculate for each sphere the maximun value of the surface field by standard routines of minimization of multivaried functions [18].

3. Disordered distribution of spheres

In this section we present numerical results corresponding to thin rectangular samples of a great number of microspheres disorderedly suspended in paraffin wax, with the external magnetic field applied in the direction normal to the sample.

We simulate this situation by placing at random the desired number of spheres in a box of dimensions $L \times L \times fL$. The form factor f is a relevant geometrical parameter since the system has scale invariance. In our studies we have employed $f = 0.1$ and 0.2. To define the geometry of the sample it is also necessary the filling factor ρ which is equal to the volume fraction occupied by the spheres. We have performed calculations for $\rho = 0.01, 0.025, 0.05, 0.10, 0.15$ and 0.20. For each case we have generated configurations with N ranging from 10 to either 100 or 150.

In analyzing such a disordered system, one must be aware of the fact that the number of spheres that can be employed in a simulation (and therefore the length of the system for fixed ρ) is much lower than what one really has in the experimental system. In this situation two points become important. First, there could be finite-size effects. This is very likely to occur because the involved interactions are long-ranged. In this case one should work with systems as large as possible, and perform some kind of extrapolation to infinite-sized systems. Secondly, statistical uncertainty is present, so in principle it is necessary to perform in each case several runs with independent configurations. This permits an estimate of the statistical errors. We expect these errors to become negligible for large systems, because experimental results turn out to be fairly reproducible [17]. In this study our objective has mainly been to show the capabilities of the numerical method, and we have limited ourselves to a simple analysis of several situations. Therefore, we have not done an exhaustive finite-size or statistical analysis, which would have been beyond the scope of the paper.

In Fig. 2, we present typical results for the distribution of maximum surface fields by varying the number of spheres employed in the simulation, for the cases of $\rho = 0.01$ and 0.20. In the most diluted case (Fig. 2a) it can be seen that the distribution is very narrow, with a high fraction of spheres having values of $B_{\max}$ very close to the value corresponding to an isolated sphere $\frac{3}{2}B_{\text{ext}}$. There appear also some couples of spheres with quite large (and very similar) maximum field; we have checked that these correspond to spheres that have been placed very close to each other, with a gap between them of

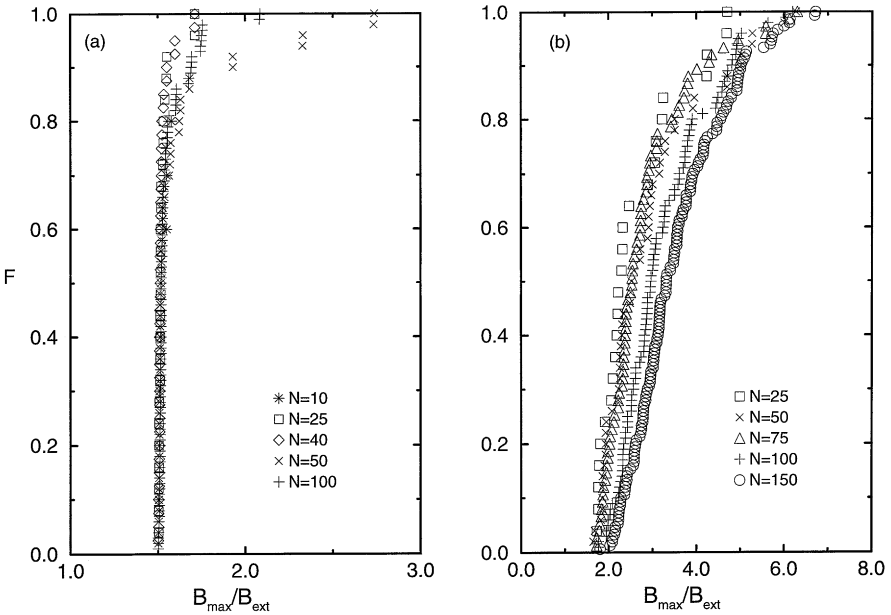

Fig. 2. Fraction F of spheres with maximum surface field lower than the x-axis value (in units of B_{ext}) for disordered configurations with several values of N. (a) $\rho = 0.01$; (b) $\rho = 0.20$.

order 0.1 times the radius or smaller, which generates strong local fields. In the more concentrated case (Fig. 2b) we see that the maximum fields take much larger values, and that the distribution is broader. On the other hand there appears a clear dependence on N, with a tendency to reach greater maximum fields as N increases.

This effect can be seen in more detail by calculating some statistical properties of the distributions of B_{max}. In Fig. 3 we show the mean of B_{max} (hereafter field values will be represented in units of B_{ext}) as a function of $1/N$ for $\rho = 0.01$ and 0.20. As expected the field values show a strong dependence on N for the largest filling factor, and only an extrapolation for $1/N \to 0$ would in principle permit a result for an infinite system. In the same figure, the standard deviation of B_{max} is also shown. For the larger ρ, the variances are larger, fluctuating around a roughly constant value.

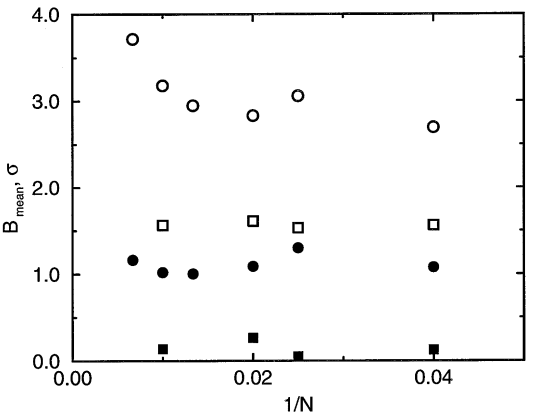

Fig. 3. Mean value (empty symbols) and standard deviation (full symbols) of the distribution of B_{max}/B_{ext} versus $1/N$ (disordered configurations). Squares: $\rho = 0.01$; Circles $\rho = 0.20$.

More interesting are the results for higher moments of the distribution, which surprisingly show a stronger dependence on N for dilute systems. In Fig. 4 we show the skewness and kurtosis of B_{max} for the same filling factors. For the *smaller* ρ, the variability of these quantities is larger than in the most dense system. In particular, the kurtosis presents a clear increase with N, and we cannot exclude the posibility of a diverging value for an infinite system. However, for the largest filling factor these values are nearly constant and very

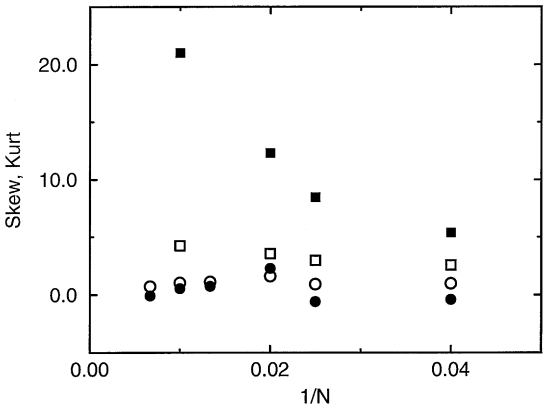

Fig. 4. Skewness (empty symbols) and kurtosis (full symbols) of the distribution of B_{max}/B_{ext} versus $1/N$ (disordered configurations). Squares: $\rho = 0.01$; Circles $\rho = 0.20$.

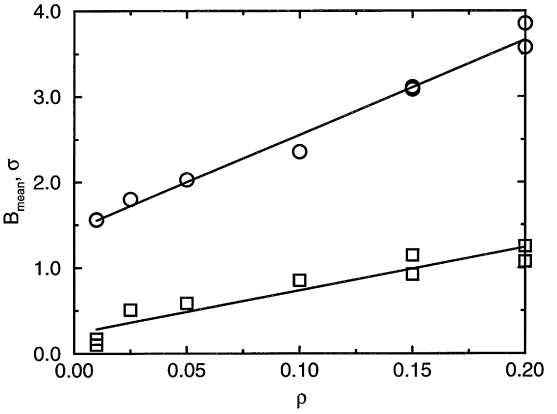

Fig. 6. Mean value (circles) and standard deviation (squares) of the distribution of B_{max}/B_{ext} versus ρ (disordered configurations).

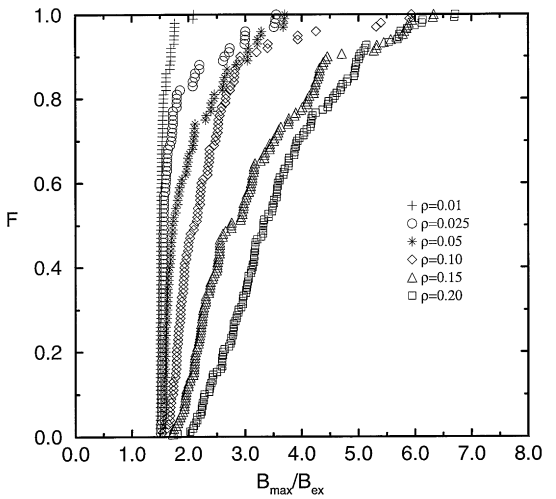

Fig. 5. Fraction F of spheres with maximum surface field lower than the x-axis value (in units of B_{ext}) for disordered configurations. $N = 100$ except for $\rho = 0.15$ and 0.20, for which $N = 150$.

close to zero, i.e. the distribution seems to be more Gaussian.

In Fig. 5 we present the distribution of maximum surface fields for several values of the filling factor, and for the greatest N employed in each case ($N = 100$ for smaller ρ and $N = 150$ for $\rho = 0.15$ and 0.20). The distribution tends to broaden and shift to higher field values as ρ increases. This can be seen in Fig. 6, where we plot the mean and the standard deviation of B_{max}. In order to estimate the statistical uncertainty, we have employed two independent configurations for each $\rho = 0.01$, 0.15 and 0.20. The mean of B_{max} presents a fairly linear behaviour in ρ over the range of filling factors employed in the simulations. A mean-squares fitting of the data gives the result

$$\frac{B_{max}}{B_{ext}} = 11.12\rho + 1.44. \tag{3.1}$$

For the standard deviation, the results are quite similar with a roughly linear dependence on ρ. An analogous fitting results in

$$\frac{\sigma}{B_{ext}} = 5.02\rho + 0.24. \tag{3.2}$$

As shown in Fig. 6, independent simulations with different configurations can present a certain degree of variability for these quantities, especially for high filling factors. Therefore only improving statistics with more simulations would permit one to obtain definitive results. In Fig. 7 the values of the skewness and the kurtosis of the distribution are represented as functions of ρ. Both quantities show a fast decay to small values as ρ reaches values of order 0.1. In particular, the kurtosis is very close to zero and the skewness only slightly greater, with very small statistical uncertainty. Therefore, we conclude that for such dense systems the distributions of maximum surface fields are

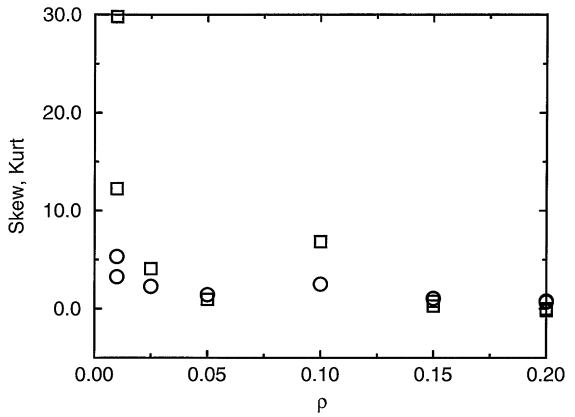

Fig. 7. Skewness (circles) and kurtosis (squares) of the distribution of B_{max}/B_{ext} versus ρ (disordered configurations).

clearly Gaussian. It is worthwhile to note the large statistical variability observed in the kurtosis for the smallest dense case.

4. Ordered distribution of spheres

We deal in this section with the case of superconducting spheres placed in regular square lattices. We will limit ourselves to planar arrays with a B_{ext} normal to the plane. Such regular configurations are not affected by disorder effects. However, as we will see below, important finite-size effects can arise in this situation.

We have performed simulations with configurations of several concentrations (i.e. several lattice spacings) and different numbers of spheres. In order to compare with disordered configurations, we have employed lattice spacing values $d/a = 7.482$, 4.376, 3.473, 3.034, and 2.757, which would correspond for tridimensional lattices to the filling factors values 0.01, 0.05, 0.10, 0.15 and 0.20, already used in the previous section. We will refer in some cases to these equivalent filling factor values, especially when comparing to disordered configurations.

Results for very dilute systems turn out to be not very interesting, because in such regular configurations the spheres are very far away from any other and the surface fields are nearly the same as on isolated spheres. However, when the concentration of spheres is increased, a broad distribution of maximum surface fields appears with noticeable finite-size effects. This can be seen in Fig. 8, where the distribution of B_{max} is shown for several values of N and for filling factors $\rho = 0.01$, 0.1 and 0.2.

The distributions for $\rho = 0.1$ and 0.2 are clearly different from those obtained in disordered configurations. First, it is obvious that in such regular lattices there are several sets of equivalent positions, and hence with the same values of B_{max}, which gives a discontinous appearance to the shapes of these curves. This effect is stronger for small lattices, where due to symmetry reasons only a few maximum values of the surface field are possible. Secondly, the distributions are very asymmetrical, with a tendency for B_{max} to assume values close to the largest, and with strong finite-size effects. We can explain these features by analyzing what happens in a large system and comparing it to an infinite system. In an infinite planar lattice, all the field lines have to pass between the spheres, and all spheres have a high value of the maximum surface field. However, for a finite system most of the field lines can easily round the sample, and the surface fields turn out to be distinctly smaller than in the infinite system. This is a manifestation of the known fact that diamagnetic interactions are long range. On the other side, spheres close to the boundaries have surface field values much smaller than in the central positions, where the field values are more similar. Spatial distributions of the maximum field values are shown in Fig. 9 for $\rho = 0.1$ and 0.2. Since there are a lesser number of positions close to the boundaries, the resulting distribution of surface fields is biased towards the greatest value.

These features can be seen in Fig. 10, where we plot the mean value of B_{max} versus $1/N$. We see that the effects of the size are important for both $\rho = 0.1$ and 0.2. Also in this figure, we display the *maximum value* of B_{max} for each ensemble of N spheres. In fact this corresponds to the value of B_{max} for the spheres placed in the middle of the system. We see that these values also show a strong dependence on N, even for the largest sizes which have not reached their assymptotic value. Also in Fig. 9 it can be seen that the boundary effects are more important at

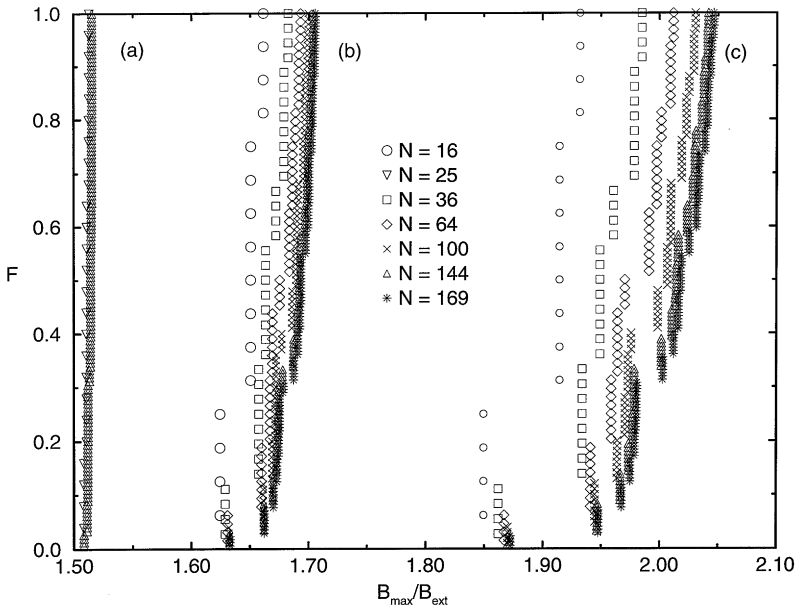

Fig. 8. Fraction F of spheres with maximum surface field lower than the x-axis value (in units of B_{ext}) for ordered configurations with several values of N. (a) $\rho = 0.01$; (b) $\rho = 0.10$; (c) $\rho = 0.20$.

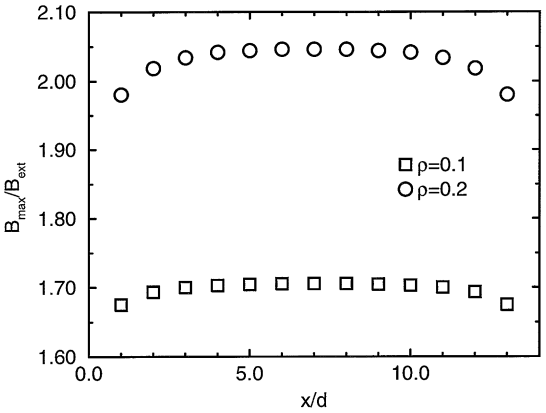

Fig. 9. Maximum surface field for spheres lying on a line crossing the square lattice in an ordered configuration. $N = 13 \times 13$.

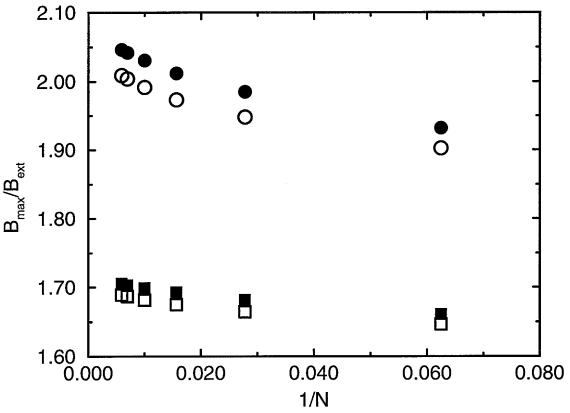

Fig. 10. Mean value (empty symbols) and maximum value (full symbols) of the distribution of B_{max}/B_{ext} versus $1/N$ (ordered configurations). Squares: $\rho = 0.10$; circles $\rho = 0.20$.

higher filling factors. On the contrary, for more diluted systems the values of maximum fields are more similar.

In Fig. 11 we show the standard deviations of B_{max} as a function of $1/N$ for $\rho = 0.1$ and 0.2. As expected, these values are much smaller than in the disordered case. It can also be seen that this function possesses a maximum for N of order 10^2. For larger values of N, a growing proportion of spheres belongs to the central region, with very similar field values, and therefore smaller deviations.

The calculation of the skewness and kurtosis of the distributions of B_{max}, shown in Fig. 12, gives

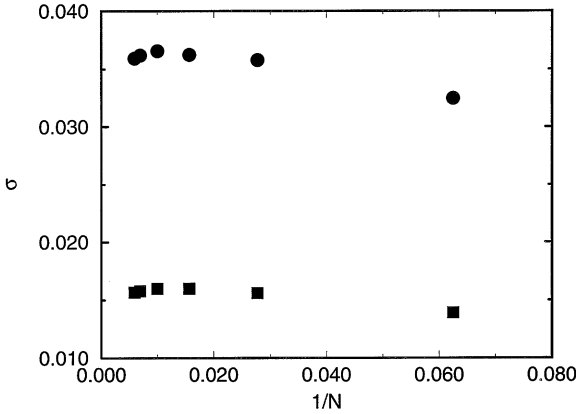

Fig. 11. Standard deviation of the distribution of B_{max}/B_{ext} versus $1/N$ (ordered configurations). Squares: $\rho = 0.10$; circles $\rho = 0.20$.

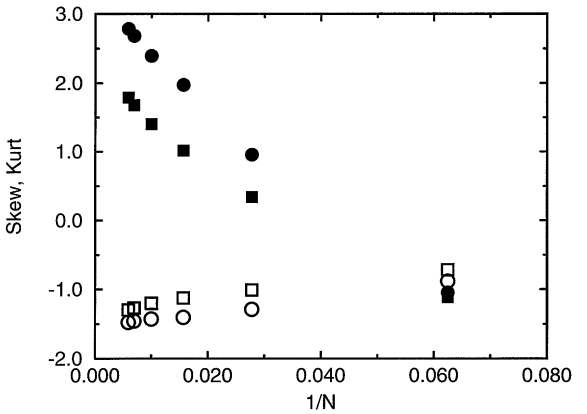

Fig. 12. Skewness (empty symbols) and kurtosis (full symbols) of the distribution of B_{max}/B_{ext} versus $1/N$ (ordered configurations). Squares: $\rho = 0.10$; circles $\rho = 0.20$.

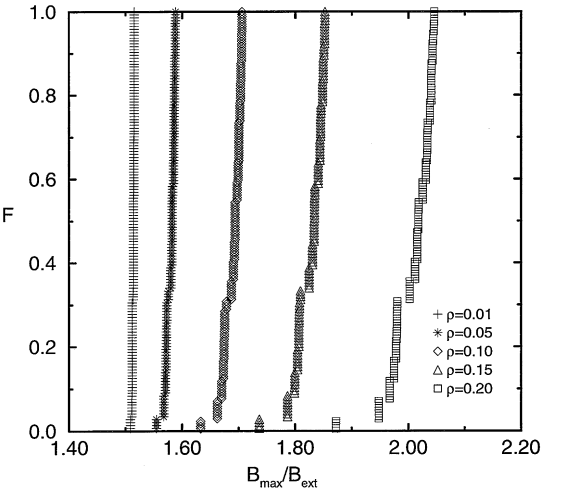

Fig. 13. Fraction F of spheres with maximum surface field lower than the x-axis value (in units of B_{ext}) for ordered configurations. $N = 144$ except for $\rho = 0.10$ and 0.20, for which $N = 169$.

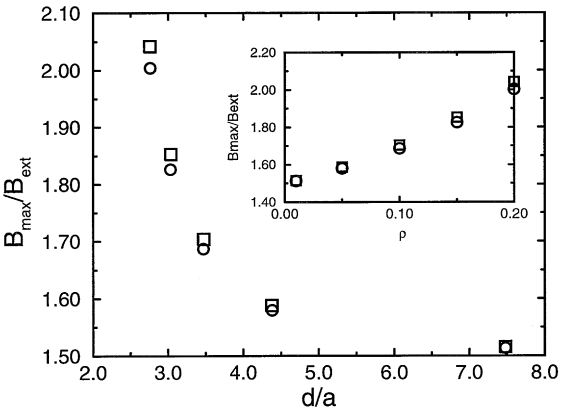

Fig. 14. Mean value (circles) and maximum value (squares) of the distribution of B_{max}/B_{ext} versus the lattice spacing. In the inset there are represented the same quantities versus ρ.

results qualitatively very different from that of the disordered distributions. The most remarkable fact is that in these regular configurations the distributions are distinctly not Gaussian even for the highest filling factors. The values of the skewness and kurtosis are very different from zero, and their absolute values tend to increase with N. As in the most diluted disordered case, the kurtosis seems to diverge in the large N limit.

The distributions of maximum surface fields for different lattice spacings are shown in Fig. 13 for the largest systems simulated. The shape of these distributions does not present great qualitative changes with increase of the filling factor. However, the field values and the width of the distributions show a strong increase with ρ. In Fig. 14 we have represented the means of the distributions of maximum surface fields and the maximum of each distribution (i.e. those corresponding to spheres located in the middle of the system) as a function of the lattice spacing. The values tend to diverge for

concentrated systems as in the disordered cases. We see a similar behaviour of the standard deviation, which we represent in Fig. 15 for the same distributions.

In Fig. 16 we show the values of the kurtosis and the skewness for the largest systems as a function of the lattice spacing. Again, results for these quantities turn out to behave in an opposite fashion to those of the disordered configurations. In particular, both absolute values increase with concentration. Moreover the kurtosis seems to diverge. We conclude that, for ordered configurations, the non-Gaussianity of the distribution of maximum fields is higher for more concentrated systems.

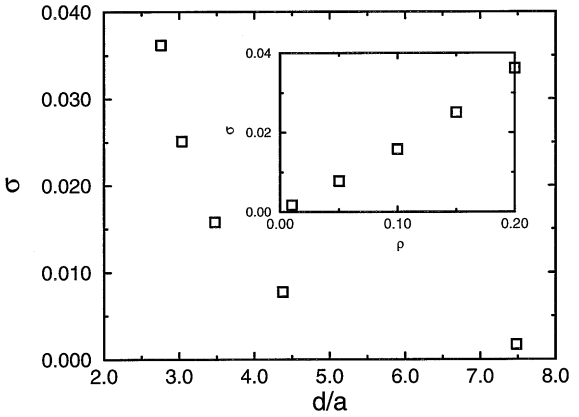

Fig. 15. Standard deviation of the distribution of B_{max}/B_{ext} versus the lattice spacing. In the inset there are represented the same quantities versus ρ.

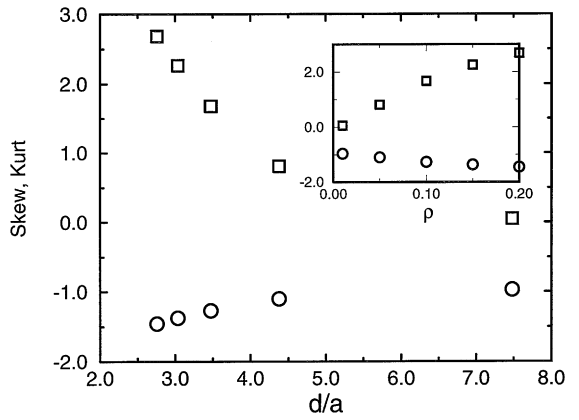

Fig. 16. Skewness (circles) and kurtosis (squares) of the distribution of B_{max}/B_{ext} versus the lattice spacing. In the inset there are represented the same quantities versus ρ.

5. Conclusions

In this paper we have implemented a numerical method to solve the Laplace equation for the magnetic field in the presence of an ensemble of diamagnetic spheres, and we have applied this method in order to find the maximum surface field on the spheres. This calculation has been motivated by experiments involved in the development of superheated superconducting granule detectors. This also should be useful in other physical situations, like the flux of a viscous fluid through a disordered medium.

The numerical procedure consists of multipole expansions of the magnetic field in the neighbourhood of each sphere and a matching of all of them by an iterative method. We have presented results for disordered and ordered configurations of superconducting spheres, and we have calculated the statistical properties of the distribution of maximum surface fields. We have studied the changes by varying the number and the concentration of spheres. We have found important finite-size effects, and a suitable $n \to \infty$ limit should be necessary for precise comparison to experiments with a high number of spheres. An important issue is the Gaussianity of the maximum surface-field distribution. For disordered configurations the field distribution appears Gaussian for high concentrations. On the contrary, ordered configurations present non-Gaussian field distributions, especially for the highest concentrations. As a final conclusion, the direct numerical resolution of the Laplace equation appears as a feasible and promising tool for performing simulations of SSG detectors.

Acknowledgements

We acknowledge T. Girard for helpful discussions and a careful correcting of the manuscript. L.R.-P. acknowledges G. Waysand, O. Heres and V. Jeudy for helpful discussions. We acknowledge

financial support from Dirección General de Investigación Científica y Técnica (Spain) (Projects PB96-0241-C02-02 and PB95-0884) and European Commision (Project TMR-ERB4061PL951377). We also acknowledge computing support from Fundació Catalana per a la Recerca-Centre de Supercomputació de Catalunya (Spain).

References

[1] T.A. Girard et al., Nucl. Instr. and Meth. A 370 (1996) 223.
[2] M. Abplanalp et al., Nucl. Instr. and Meth. A 370 (1996) 227.
[3] A.K. Drukier, C. Vallete, Nucl. Instr. and Meth. 105 (1972) 285.
[4] A.K. Drukier, Nucl. Instr. and Meth. 173 (1980) 259.
[5] A.K. Drukier, Nucl. Instr. and Meth. 201 (1982) 77.
[6] A.K. Drukier, C. Valette, G. Waysand, L.C.L. Yuan, F. Peters, Lett. Nuovo Cimento 14 (1975) 300.
[7] J. Blot, Y. Pelan, J.C. Pineau, J. Rosenblatt, J. Appl. Phys. 45 (1974) 1429.
[8] J. Behar, J.M. Cardi, B. Herszberg, D. Hueber, C. Valette, G. Waysand, J. Phys. (Paris) 39 (1978) C6–1201.
[9] A.K. Drukier, J. Igalson, L. Sniadower, Nucl. Instr. and Meth. 154 (1978) 91.
[10] A.K. Drukier, L.C.L. Yuan, Nucl. Instr. and Meth. 138 (1976) 213.
[11] L. Gonzales-Mestres, D. Perret-Gallix, Nuovo Cimento C 9 (1986) 573.
[12] M. Le Gros, A. Da Silva, B.G. Turrell, A. Kotlicki, A.K. Drukier, Appl. Phys. Lett. 56 (1990) 2234.
[13] C. Valette, G. Waysand, D. Stauffer, Solid State Commun. 41 (1982) 305.
[14] M. Hillen, D. Stauffer, Solid State Commun. bf 43 (1982) 487.
[15] U. Geigenmüller, J. Phys. (Paris) 49 (1988) 405.
[16] U. Geigenmüller, in: (Eds.), G. Waysand, G. Chardin Superconducting and Low-Temperature Particle Detectors, Elsevier, Amsterdam, 1989 [there are some minor typos in Eqs. (3.14), (3.16) and (3.17)].
[17] V. Jeudy, D. Limagne, G. Waysand, Nucl. Phys. B (Proc. Suppl.) 28A (1992) 482.
[18] W.H. Press, S.A. Teukolsky, W.T. Vetterling, B.P. Flannery, Numerical Recipes, 2nd ed., Cambridge University Press, Cambridge, 1992.